Hydrology and
Earth System
Sciences

Open Access

Estimates of global dew collection potential on artificial surfaces

H. Vuollekoski[1], **M. Vogt**[1,2], **V. A. Sinclair**[1], **J. Duplissy**[1], **H. Järvinen**[1], **E.-M. Kyrö**[1], **R. Makkonen**[1], **T. Petäjä**[1],
N. L. Prisle[1], **P. Räisänen**[3], **M. Sipilä**[1], **J. Ylhäisi**[1], **and M. Kulmala**[1]

[1]University of Helsinki, Department of Physics, Helsinki, Finland
[2]Norwegian Institute for Air Research, Oslo, Norway
[3]Finnish Meteorological Institute, Helsinki, Finland

Correspondence to: H. Vuollekoski (henri.vuollekoski@helsinki.fi)

Abstract. The global potential for collecting usable water from dew on an artificial collector sheet was investigated by utilizing 34 years of meteorological reanalysis data as input to a dew formation model. Continental dew formation was found to be frequent and common, but daily yields were mostly below 0.1 mm. Nevertheless, some water-stressed areas such as parts of the coastal regions of northern Africa and the Arabian Peninsula show potential for large-scale dew harvesting, as the yearly yield may reach up to $100 \, \mathrm{L\,m^{-2}}$ for a commonly used polyethylene foil. Statistically significant trends were found in the data, indicating overall changes in dew yields of between $\pm 10\,\%$ over the investigated time period.

1 Introduction

The increasing concern over the diminishing and uneven distribution of fresh water resources affects the daily life and even survival of billions of people. The United Nations Development Programme (2006) estimated that there were already 1.1 billion people in developing countries lacking adequate access to water, a figure that is expected to climb to 3 billion by 2025 due to the increasing population particularly in the most water-stressed parts of the planet.

On the other hand, water exists everywhere in one form or another: ground water, rivers, lakes, seas, glaciers, snow, ice caps, clouds, soil, and as air moisture. In particular, air moisture is present everywhere; even the driest of deserts have some, and warm air can contain more humidity than cold air. The absolute quantities of water by volume of air are of course very small (of the order of grams or some tens of

grams per cubic metre), and harvesting it may be expensive or technologically demanding – factors that are rarely met in the areas of most immediate need for sustainable sources of water. Nevertheless, if no other sources of usable water exist nearby, harvesting water from the air might provide an economically sound supply of water for both drinking and agriculture.

Harvesting moisture from the air has two potential pathways: fog and dew. Fog is a highly local phenomenon that occurs, for example, when moist air is cooled by the emission of long-wave radiation or by forced ascent up a mountain slope: the decrease in temperature causes supersaturation and the formation of fog. The droplets may then be harvested by artificial structures resembling tennis nets equipped with rain gutters as has been investigated in many previous studies (e.g. Schemenauer and Cereceda, 1991; Klemm et al., 2012; Fessehaye et al., 2014).

The formation of dew occurs when the temperature of a surface is below the dew point temperature, and water vapour condenses onto the surface. In this study, the surface is assumed to be a macroscopic, artificial structure. Since only a thin layer of air over the surface reaches supersaturation, by volume the formation of dew is a very slow process compared to the formation of fog. Nevertheless, the formation and collection of dew has been studied and has been found to be feasible in several locations around the world (e.g. Nilsson, 1996; Zangvil, 1996; Kidron, 1999; Jacobs et al., 2000; Beysens et al., 2005; Lekouch et al., 2012). Additionally, material design can affect the characteristics of the condensing surface and improve its efficiency for dew collection. For example, the higher the emissivity of the surface, the higher its rate of cooling by radiation. During nights with clear skies,

when both sunlight and thermal radiation from clouds are absent, the incoming radiation may be exceeded by the device's own out-going thermal radiation, resulting in a net cooling.

In this global modelling study we focus on the formation of dew onto an artificial surface, and investigate the potential for its collection. This seemingly arbitrary limitation is based on the following facts: (a) the potential for dew formation is almost ubiquitous regardless of orographic features or presence of water in other forms, (b) the formation of dew can be artificially enhanced with relatively minor efforts, (c) the formation of dew is a well-defined mathematical problem suitable for computer modelling at global scales, and (d) we are unaware of any such previous studies.

This paper describes the implementation of a model for dew formation onto an artificial surface, which is upscaled with meteorological input from a long-term reanalysis data set that spans the years 1979–2012. Modelling 34 years of dew formation ensures that the results are statistically robust. Our approach is based on an energy balance model similar to those in e.g. Nilsson (1996), Madeira et al. (2002), Beysens et al. (2005), Jacobs et al. (2008), Richards (2009) and Maestre-Valero et al. (2011), who have demonstrated that their models are able to predict the measured dew yields within reasonable accuracy.

The dew formation model, forced with reanalysis data, provides spatially coarse (80 km) estimates of dew collection yields for given sheet technologies along with the temporal evolution of dew formation. Therefore, the model output allows global maps of dew formation to be produced and areas with potential for large-scale dew collection to be identified. The modelled dew collection estimates can be used as first-order estimates by those who are planning local feasibility studies that include additional factors such as lakes, rivers, and road access. The long time series of our study provides information about the seasonal variation of dew formation as well as long-term trends in dew yield, which could be associated with climate change.

2 Methods

In order to form global estimates of dew collection potential, we combined a computationally efficient dew formation model with historical, global meteorological reanalysis data spanning 34 years. The offline model was run on a computer cluster with 128 cores, which allowed global model runs with different parameterizations to be run in approximately 24 h each.

The program source code, written in Python and Cython, is available at https://github.com/vuolleko/dew_collection/.

2.1 Model description

In implementing the model that describes the formation of dew (represented by mass yield of either liquid water or ice),

Table 1. Some parameters used in the model, unless specified otherwise. The properties of the foil are for common low-density polyethylene with composition according to Nilsson et al. (1994) and radiative properties as found by Clus (2007).

Parameter	Value
Sheet density ρ_c	$920 \, \mathrm{kg \, m^{-3}}$
Sheet thickness δ_c	$0.39 \, \mathrm{mm}$
Sheet specific heat capacity C_c	$2300 \, \mathrm{J \, kg^{-1} \, K^{-1}}$
Sheet IR emissivity e	0.94
Sheet short-wave albedo a	0.84
Time step	$10 \, \mathrm{s}$

we followed the approach presented by Pedro and Gillespie (1982) and Nikolayev et al. (1996), which has been found to agree reasonably well with empirical measurements of dew collection (e.g. Nilsson, 1996; Beysens et al., 2005; Jacobs et al., 2008; Richards, 2009; Maestre-Valero et al., 2011). The algorithm integrates the prognostic equations for the mass and heat balance by turns, thereby describing the temperature of the condenser and the resulting condensation rate onto it. As the model is global and thus incorporates both polar regions, we include the dynamics of water changing phase between liquid and solid. However, for simplicity, here we refer to both phase changes of vapour-to-liquid (condensation) and vapour-to-ice (desublimation) as condensation, and to both liquid and solid phases as water, unless specified otherwise. In our model we consider dew only and the occurrence of precipitation or fog are unaccounted for apart from their potential indirect effects included within the input reanalysis data.

The condenser in our model is a horizontally aligned sheet of some suitable material, such as low-density polyethylene (LDPE) or polymethylmethacrylate (PMMA), and is thermally insulated from the ground at a height of 2 m. Unless specified otherwise, the particular parameter values used in the model (listed in Table 1) match those of the inexpensive LDPE foil used by e.g. the International Organization for Dew Utilization, whose foil composition follows Nilsson et al. (1994).

The heat equation can be written as

$$\frac{dT_c}{dt}(C_c m_c + C_w m_w + C_i m_i) = P_{rad} + P_{cond} + P_{conv} + P_{lat}, \quad (1)$$

where T_c, C_c, and m_c are the condenser's temperature, specific heat capacity and mass, respectively. The condenser's mass is given by $m_c = \rho_c S_c \delta_c$, where ρ_c, S_c and δ_c are its density, surface area (here $1 \, \mathrm{m^2}$) and thickness (see Table 1). C_w and m_w are the specific heat capacity and mass of liquid water, representing the cumulative mass of water that has condensed onto the sheet, whereas C_i and m_i are the respective values for ice.

The right-hand side of Eq. (1) describes the powers involved in the heat exchange processes. The radiation term,

Original parameter	Derived model input
10 metre U wind component	
10 metre V wind component	Wind speed
Forecast surface roughness	
2 metre temperature	Air temperature
2 metre dew point temperature	Dew point
Surface solar radiation downwards	Short-wave radiation in
Surface thermal radiation downwards	Long-wave radiation in

P_{rad}, consists of three parts:

$$P_{rad} = (1-a)S_c R_{sw} + \varepsilon_c S_c R_{lw} - P_c, \tag{2}$$

where R_{sw} and R_{lw} are the solar and thermal components of the incoming radiation from the input reanalysis data (see Table 2), a is the sheet's albedo and ε_c its emissivity (i.e. the absorbed fraction of radiation) in the infra-red band. Note that the effect of cloudiness is indirectly included via the input radiation terms. The outgoing radiative power, P_c, is given by the Stefan–Boltzmann law,

$$P_c = S_c \varepsilon_c \sigma T_c^4, \tag{3}$$

where σ is the Stefan–Boltzmann constant.

Returning to Eq. (1), the term P_{cond} describes the conductive heat exchange between the condenser surface and the ground. For simplicity, we assume perfect insulation, and the term vanishes.

The convective heat-exchange term, P_{conv}, is given by

$$P_{conv} = S_c h (T_a - T_c), \tag{4}$$

where T_a is the 2 m ambient air temperature and h is the heat transfer coefficient, estimated by a semi-empirical equation (Richards, 2009):

$$h = 5.9 + 4.1u \frac{511 + 294}{511 + T_a} \tag{5}$$

in units $W\,K^{-1}\,m^{-2}$, where u is the prevailing 2 m horizontal wind speed. However, for convenience, the model accepts any parameterization of the heat transfer coefficient (in functional form) as a model input parameter. Please see Sect. 2.3 for more details on the heat transfer coefficient.

The final term in Eq. (1), P_{lat}, represents the latent heat released by the condensation/desublimation of water

$$P_{lat} = \begin{cases} L_{vw} \frac{dm_w}{dt} & \text{if } T_c \geq 0°C \\ L_{vi} \frac{dm_i}{dt} & \text{if } T_c < 0°C, \end{cases} \tag{6}$$

where L_{vw} and L_{vi} are the specific latent heat of vaporization and desublimation for water, the appropriate one selected

based on whether the temperature of the condenser is above or below the freezing point of water. The algorithm imposes a similar condition for dynamically changing the phase of pre-existing water or ice on the condenser sheet: if liquid water exists (i.e. $m_w > 0$) while $T_c < 0$ and the sheet is losing energy (i.e. the right-hand side of Eq. 1 is negative), instead of solving Eq. (1), the model will keep T_c constant and solve

$$L_{wi} \frac{dm_w}{dt} = P_{rad} + P_{conv} + P_{lat}, \tag{7}$$

where L_{wi} is the latent heat of fusion. The mass of lost (i.e. frozen) water is added to the cumulated mass of ice. A similar equation is solved for m_i in situations when there is ice present on the condenser but the temperature of the condenser is above zero degrees Celsius. Note that Eq. (7) is unrelated to condensation, and only describes the phase transition of already condensed water or ice.

For the rate of condensation (independent of Eq. 7) we can write a mass balance equation

$$\frac{dm}{dt} = \max(0, S_c k (p_{sat}(T_d) - p_c(T_c))), \tag{8}$$

where m represents either m_i or m_w depending on whether $T_c < 0°C$ or not, $p_{sat}(T_d)$ is the saturation pressure at the dew point temperature, $p_c(T_c)$ is the vapour pressure over the condenser sheet and k is the mass transfer coefficient, defined through the heat transfer coefficient (Eq. 5)

$$k = \frac{h}{L_{vw}\gamma} = \frac{0.622h}{C_a p}, \tag{9}$$

where γ is the psychrometric constant, p is the atmospheric air pressure and C_a is the specific heat capacity of air. Note that Eq. (8) assumes irreversible condensation, i.e. there is no evaporation or sublimation during daytime even when $T_c > T_a$. This assumption simulates the daily manual collection of the condensed water around sunrise, soon after which the temperature of the sheet often increases above the dew point temperature. In the model we reset the cumulated values for water and ice at local noon, and take the preceding maximum value of $m_w + m_i$ as the representative daily yield.

In our model we approximate the vapour pressure $p_c(T_c)$ in Eq. (8) by the saturation pressure of water at temperature T_c. In reality, the wettability of the surface affects the vapour pressure p_c directly above it: a wetted surface decreases the vapour pressure, and condensation may take place even if $T_c > T_d$ (Beysens, 1995). Beysens et al. (2005) accounted for this effect by including an additional empirical parameter, T_0, such that $p_c(T_c) = p_{sat}(T_c + T_0)$, and found the optimal value of T_0 to be -0.35 K. However, Beysens et al. (2005) used a collector with a different design to that assumed in this study, a more expensive, 5 mm thick PMMA plate, and we were unable to find a reference value for T_0 valid for LDPE. We thus set $T_0 = 0$. This simplification causes a small underestimation of the condensation rate calculated by Eq. (8).

www.hydrol-earth-syst-sci.net/19/601/2015/
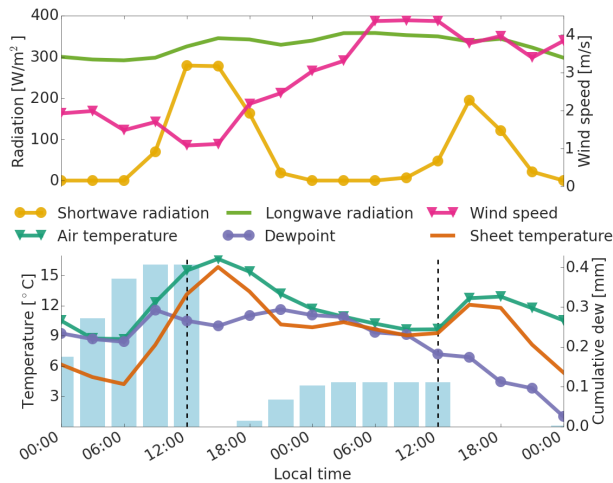
Hydrol. Earth Syst. Sci., 19, 601–613, 2015

Figure 1. An example of modelled dew formation events on two consecutive days in September 2000 in Helsinki, Finland. The short-wave and long-wave radiation, wind speed, air temperature and dew point are input from the ERA-Interim data set. Note that the cumulated amount of dew (vertical bars) is reset daily at local noon (dashed vertical lines). All data are in 3 h resolution.

The model reads all input data for a given grid point and solves Eqs. (1), (7) and (8) using a fourth-order Runge–Kutta algorithm with a 10 s time step. An example case spanning two consecutive days is presented in Fig. 1, which shows the long- and short-wave radiation components, wind speed, air temperature, dew point temperature as well as the modelled sheet temperature and cumulated dew. During daytime, the incoming short-wave radiation from the sun as well as the atmospheric long-wave radiation act to increase the temperature of the condenser sheet. In contrast, during dark periods, the outgoing thermal radiation exceeds the atmospheric long-wave radiation, the latter of which is greatly influenced by cloudiness: the thermal emission by clouds, especially low clouds, increases the incoming thermal radiation at the surface. As condensation occurs when the temperature of the condenser sheet is below the dew point temperature (Eq. 8), significant dew cumulation can only occur during night-time. The daily collection of dew occurs at noon, depicted by the dashed vertical lines.

2.2 Meteorological input data

The meteorological input data for the dew formation model is obtained from the European Centre for Medium Range Weather Forecasts (ECMWF) Interim Reanalysis (ERA-Interim, Dee et al., 2011). Such reanalysis data sets are produced by combining historical observations from multiple sources with a comprehensive numerical model of the atmosphere using data assimilation systems. As numerical models of the atmosphere are constantly evolving, reanalysis data sets are more appropriate for long-term studies than operational analyses as a fixed numerical model is used. Numer-

ous different global reanalysis data sets are available, for example NASA MERRA (Rienecker et al., 2011), JRA-25 (Onogi et al., 2007) and NCEP-CFSR (Saha et al., 2010), and many inter-comparison studies between the different reanalysis data sets have been conducted (e.g. Lorenz and Kunstmann, 2012; Willett et al., 2013; Simmons et al., 2014). ERA-Interim was selected for this study primarily because it is the only available reanalysis which assimilates two-metre temperature and therefore has a lower two-metre temperature bias than any other available re-analysis (Decker et al., 2012).

ERA-Interim is ECMWF's current global reanalysis data set spanning 1979–present which has a horizontal resolution of $0.75°$ (approximately 80 km) and 60 levels in the vertical. We use 34 years (1979–2012) of ERA-Interim data and the variables extracted from ERA-Interim to be applied in the dew formation model are listed in Table 2. The data for wind speed, temperature and dew point temperature originate from reanalysis fields valid at 00:00, 06:00, 12:00 and 18:00 UTC, while the data valid at 03:00 and 09:00 UTC (15:00 and 21:00 UTC) are forecast fields based on the reanalysis of 0:00 UTC (12:00 UTC). The radiative parameters are purely forecast fields and are cumulative over the forecast period; in this study we derive a simple average from the difference between adjacent cumulative values to obtain instantaneous values.

The dew formation model requires the wind speed at a height of two metres, whereas only the 10 m wind speed is available in the ERA-Interim reanalysis data set. Therefore, the 2 m wind speed is estimated using the logarithmic wind profile (e.g. Seinfeld and Pandis, 2006) in the positive-definite form

$$u = \frac{\log((2 + z_0)/z_0)}{\log((10 + z_0)/z_0)} \sqrt{u_{10,x}^2 + u_{10,y}^2}, \qquad (10)$$

where z_0 is the forecast surface roughness taken from the ERA-interim reanalysis data set and $u_{10,x}$ and $u_{10,y}$ are the 10 m horizontal wind speed components.

Even by combining the ERA-Interim forecast fields with the analyses fields, the temporal resolution of the meteorological input data is only 3 hours. In contrast, the numerical dew formation model requires meteorological input every time step (10 s). Therefore, the 3-hourly ERA-Interim data is linearly interpolated to 10 s time resolution. This is a disadvantage of using reanalysis data compared to using more frequent observations. However, we believe that this disadvantage is considerably outweighed by the advantages of using reanalysis data – the long time series and the uniform global coverage. Finally, it should be emphasized that in addition to their relatively low resolution, reanalysis data sets have inherent uncertainties and they must not be regarded as exact representations of reality.
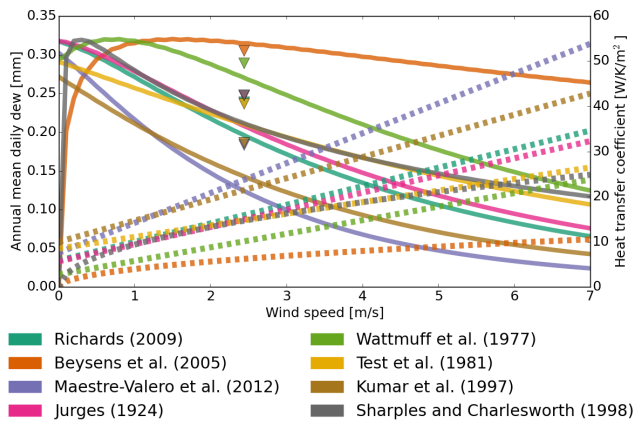
Figure 2. Sensitivity of the model to the heat transfer coefficient. The dashed lines represent heat transfer coefficients for different parameterizations as functions of wind speed. The triangles represent annual mean daily yields of dew using one year of ERA-Interim data for the grid point closest to the Negev Desert, Israel (30.75° N, 34.5° E) in 1992 (here plotted against the annual mean wind speed). The solid lines are the same, but the wind speed has been fixed according to x axis.

2.3 Transfer coefficients

In the model, the heat transfer coefficient determines how effectively the surrounding air heats or cools the condenser surface. During dew formation the surface must be cooler than the air surrounding it, which means that a high heat transfer coefficient impedes dew formation. On the other hand, the mass transfer coefficient is proportional to the heat transfer coefficient, and determines the efficiency of water vapour molecules condensing on the condenser surface. The net effect of a high heat transfer coefficient is therefore ambiguous.

The mentioned transfer phenomena can be divided into free and forced (e.g. wind-driven) convection. In wind-driven atmospheric conditions the heat transfer coefficient is often parameterized as

$$h = a + bu^n,\tag{11}$$

where a, b and n are empirical constants (possibly related to some other parameters). The constant a can be thought to correspond to free convection, although absent in some parameterizations.

Various such parameterizations (with somewhat differing assumptions) for the heat transfer coefficients can be found in the literature; Table 3 lists a few of them. Figure 2 presents these heat transfer coefficients as functions of wind speed (dashed lines). Clearly, the variance is large, especially at larger wind speeds. It should be noted that the authors of these semi-empirical parameterizations have typically assumed a quite narrow range of validity in regard to wind speed. For example, the parameterization by Richards (2009), based on McAdams (1954), is said to be valid for wind speeds $u < 5\,\mathrm{m\,s^{-1}}$. However, 3 h average wind speeds

Table 3. A selection of the various parameterizations for the heat transfer coefficient found in the literature. The first three are studies on dew formation. Here, u and T_a are the horizontal wind speed and air temperature at 2 m height, and D is the characteristic length of the condenser (e.g. 1 m).

Source	Equation
Richards (2009); this study	$h = 5.9 + 4.1u\frac{511+294}{511+T_a}$
Beysens et al. (2005)	$h = 4\sqrt{u/D}$
Maestre-Valero et al. (2011)	$h = 7.6 + 6.6u\frac{511+294}{511+T_a}$
Jürges (1924)	$h = 5.7 + 3.8u$
Watmuff et al. (1977)	$h = 2.8 + 3u$
Test et al. (1981)	$h = 8.55 + 2.56u$
Kumar et al. (1997)	$h = 10.03 + 4.687u$
Sharples and Charlesworth (1998)	$h = 9.4\sqrt{u}$

at 2 m derived from the ERA-Interim data set rarely exceed this value over continental areas.

The mass transfer coefficient is defined through the heat transfer coefficient according to Eq. (9). As noted, the effects of heat and mass transfer are opposite during dew formation.

In order to gain some estimates of the model sensitivity to the transfer coefficients, we performed several series of model runs with different parameterizations. Figure 2 presents the annual mean of the daily yield of dew in 1992 for the grid point closest to the Negev Desert, Israel. For each parameterization, the model was run once with the ERA-Interim data for the year 1992 (triangles). Next, the same model run was repeated so that the wind speed was fixed to one value for the entire year; this was repeated for all wind speeds between 0 and $7\,\mathrm{m\,s^{-1}}$ in $0.1\,\mathrm{m\,s^{-1}}$ resolution (solid lines). Altogether Figure 2 therefore presents $1 + 71$ years of simulations for each parameterization. Clearly, the difference in dew yields between the parameterizations is less pronounced than in the heat transfer coefficients alone. Nevertheless, the difference is significant, and suggests that the choice of transfer coefficients is important for model performance. Note especially the behaviour of parameterizations by Sharples and Charlesworth (1998) and Beysens et al. (2005) for pure forced convection at wind speeds close to zero.

The same test was performed for 10 locations globally (not shown), and the general characteristics are similar to those in Fig. 2, albeit a larger mean wind speed did cause more deviation in some cases.

For the global runs presented in this paper, we chose the parameterization used by Richards (2009), as this heat coefficient is close to the average presented in the literature and is well behaved also at very low wind speeds, see Fig. 2. Additionally, the study was also dedicated to dew, although the condensing surface was an asphalt-shingle roof. The dew study by Maestre-Valero et al. (2011) used the same type of foil as our virtual condenser, albeit inclined at 30°, which
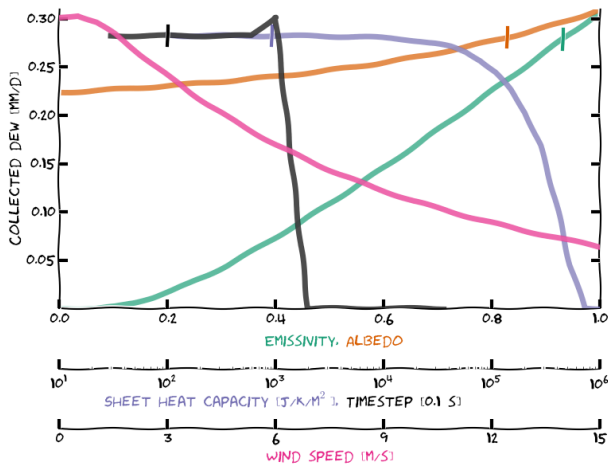
Figure 3. Sensitivity of the model to the emissivity, albedo and heat capacity of the condenser sheet as well as to the wind speed and time step of the model ($\times 10$ in figure). The heat capacity is defined here as $C_c \rho_c S_c \delta_c$, i.e. its variation corresponds to varying any of these factors. The input data correspond to Table 1 and the first day of Fig. 1, where applicable. The vertical bars represent these *default* values.

may be the reason for their significantly higher heat transfer coefficient.

For convenience, our model accepts any functional form of the heat transfer coefficient as input to the model, and several are available built-in.

3   Results and discussion

Figure 3 illustrates the sensitivity of the modelled dew yield to changes in the emissivity, albedo, and heat capacity of the sheet as well as to the wind speed and the time step of the model. The dew yield increases almost linearly with the sheet's emissivity, and the emissivity seems to be the most important factor to consider when designing condenser materials (besides economic factors). The albedo of the sheet has a smaller effect as it only affects the sheet's temperature during sunlit hours, when the sheet is anyhow heated convectively by high air temperatures (see Fig. 1). The sheet's heat capacity does not significantly affect the dew yield unless it is either very low or very high (note the logarithmic scale). Interestingly, the issue of heat capacity may have been the key limiting factor in massive ancient dew collection infrastructure (Nikolayev et al., 1996). Note that for the simulated horizontal plane, current technologies already lie close to optima. The model time step was chosen to be 10 s as this keeps the model stable even in the very-high-yield scenario of Fig. 3.

Finally, the effect of wind speed is more complex: decreasing the wind speed reduces the mass flow towards the condenser, whereas increasing the wind speed increases convective heating. It should be noted that the model formulation used in this study assumes a constant supply of atmospheric

moisture defined by the dew point temperature. In a more realistic scenario, the layer of air directly above the surface of the condenser should eventually dry if both vertical mixing and the horizontal wind speed were small, which may become important for very large collectors. On the other hand, the potential for dew collection still exists, and when designing large-scale dew collection, passive air-mixers should be introduced to ensure a supply of moist air. For model sensitivity regarding wind speed, see also Sect. 2.3 and Fig. 2.

The following results originate from a series of global simulations. The model simulations differ only by the parameters of albedo and emissivity that describe the ability of the condenser's sheet to emit and absorb energy by radiation. Recall that the spatial resolution of the meteorological input data is relatively coarse, $0.75° \times 0.75°$ (up to 80 km, depending on latitude), which does limit the model's ability to capture small-scale phenomena such as those caused by local topography. Therefore, this limitation should be considered when interpreting the model results.

Furthermore, Beysens et al. (2005) introduced additional site-specific parameters to the heat and mass transfer coefficients (Eqs. 5, 9) to accommodate for differences in environmental conditions between the condenser surface and the meteorological instruments, as well as a correction in Eq. (8) to account for surface wetting. In our study the difference between the reanalysis data and any real physical location within the area represented by the grid point could arguably be much greater than the differences considered in Beysens et al. (2005), but as we see no means to tailor the model separately for each grid point, we use the theoretical formulation as it is. This assumption will inevitably cause some error in the dew yield estimates, although the large-scale average should be reasonably well predicted.

3.1   Occurrence of dew

First and foremost, it is important to gain insight into how frequently dew forms onto the artificial surface in different areas around the world. Our model results suggest that dew formation is both global and common in continental areas, with surprisingly little seasonal variation in most areas. Figure 4 presents the mean seasonal fraction of days during which the formation of dew onto the collector occurs (i.e. the yield is positive). Apart from very warm and dry deserts, the meteorological conditions on almost all continental areas favour the formation of dew onto the collector.

The lack of dew formation is generally caused by inefficient nocturnal cooling of the surface as a result of high incoming long-wave radiation, which occurs due to a high cloud fraction and high humidity in the atmosphere (although high humidity at surface level favours dew formation).

Perhaps somewhat counter-intuitively, in general the artificial surfaces over oceans do not collect dew as regularly as those over land areas. The lack of oceanic dew formation is probably caused by higher wind speeds and the weaker diur-
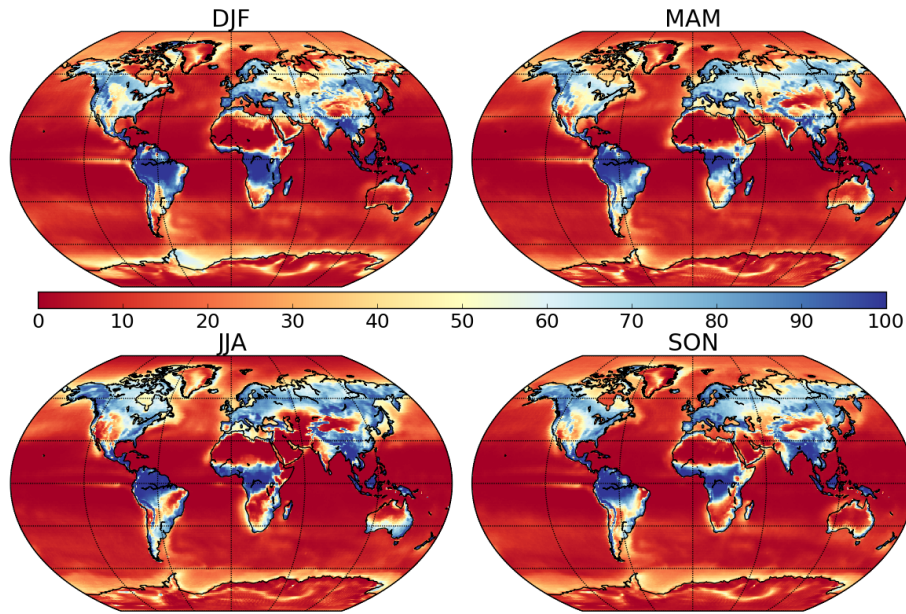
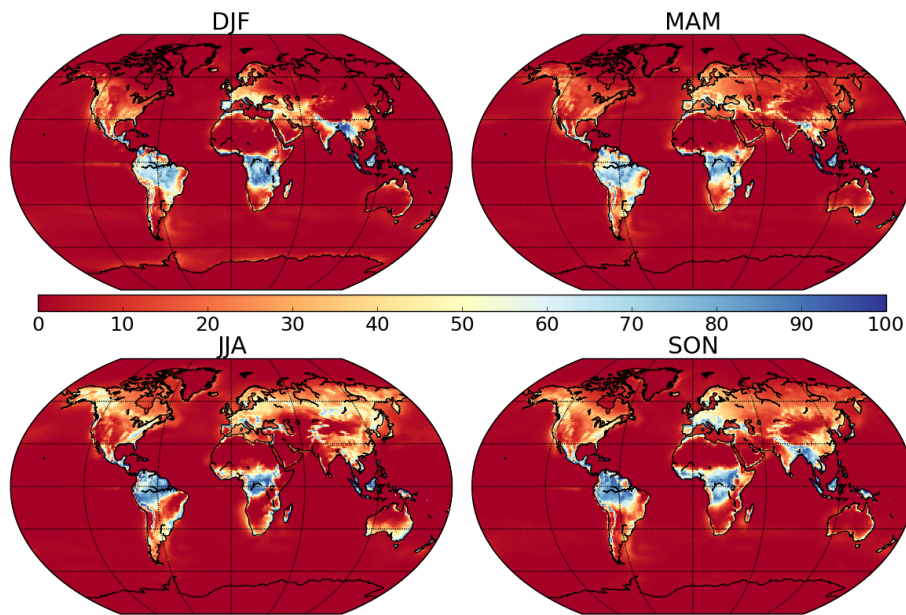**Figure 4.** Seasonal occurrence of dew as a fraction of days (%).

Figure 5. Seasonal occurrence of dew as a fraction of days (%) with a threshold of $0.1\,\mathrm{mm\,d^{-1}}$.

nal cycle in air temperature, denser average cloud cover (e.g. King et al., 2013) and higher humidity compared to land areas, resulting in amplified long-wave radiation downwards, and therefore weaker cooling.

In most dew events represented by Fig. 4, the cumulated amount of water is insignificant (see Sect. 3.2). Figure 5 shows a similar seasonal occurrence of dew as fraction of days, but only during which more than $0.1\,\mathrm{mm\,d^{-1}}$ (i.e. $0.1\,\mathrm{L\,m^{-2}\,d^{-1}}$) can be collected. The contrast between the two figures is notable, as in the latter the seasonal variation

is higher and dew formation occurs regularly in far fewer areas, most of which do not have a water shortage problem. However, in some water-stressed areas, such as the coastal regions of North Africa and the Arabian Peninsula, dew collection may be an alternative source of water worth investigating further.
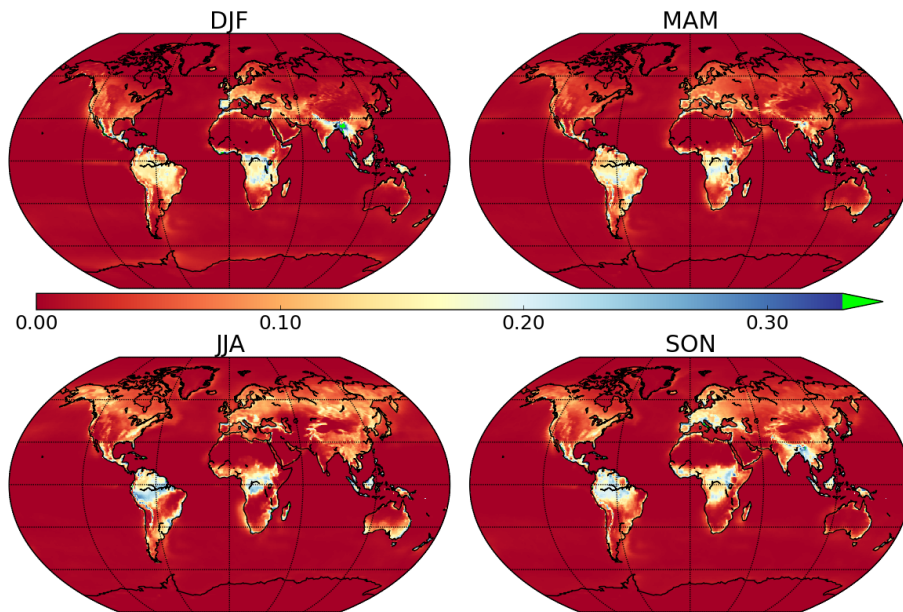
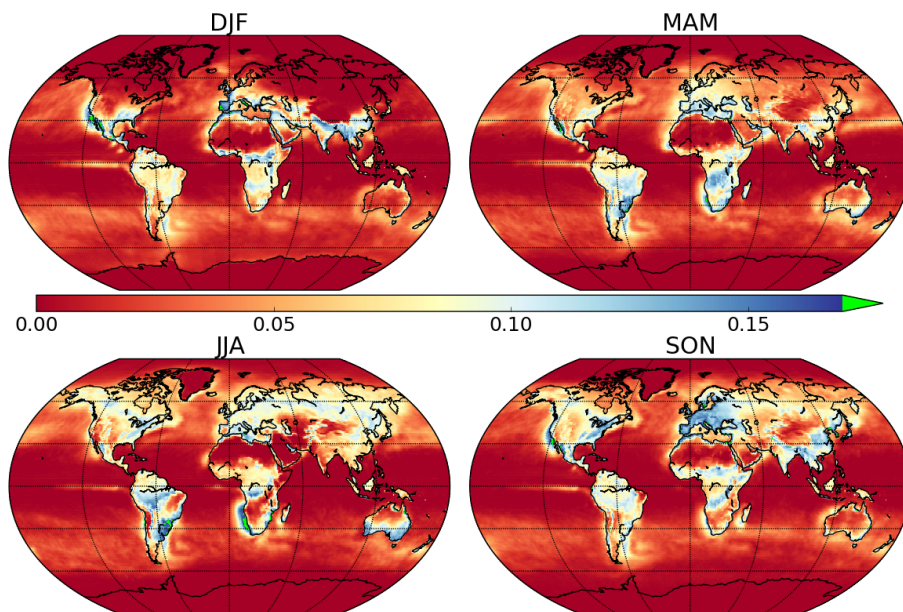**Figure 6.** Mean seasonal formation of dew (mm d^{-1}).

Figure 7. Standard deviation of the seasonal formation of dew (mm d^{-1}).

3.2 Yield of dew

Given the occurrence of dew formation events as presented in Sect. 3.1, we subsequently calculated the mean seasonal values for the actual daily amounts of dew cumulated on the collector sheet. The reported values represent the liquid water-equivalent volumes of the sum of liquid water and ice. For the condenser parameters shown in Table 1, this *dew potential* is presented in Fig. 6. Unsurprisingly, the global distribution of dew potential closely resembles Fig. 5 and indicates

that most areas with the potential to harvest non-negligible quantities of dew are also those with sufficient other sources of water. Note the high seasonal variation especially in equatorial Africa, Southeast Asia and southern Australia.

The standard deviation of the seasonal formation of dew is presented in Fig. 7. The variation is surprisingly zonal compared to Fig. 6. On the other hand, the highest variation is found in regions with the highest dew yields as might be expected. In particular, dew yields in the aforementioned coastal regions of northern Africa and the Arabian Penin-
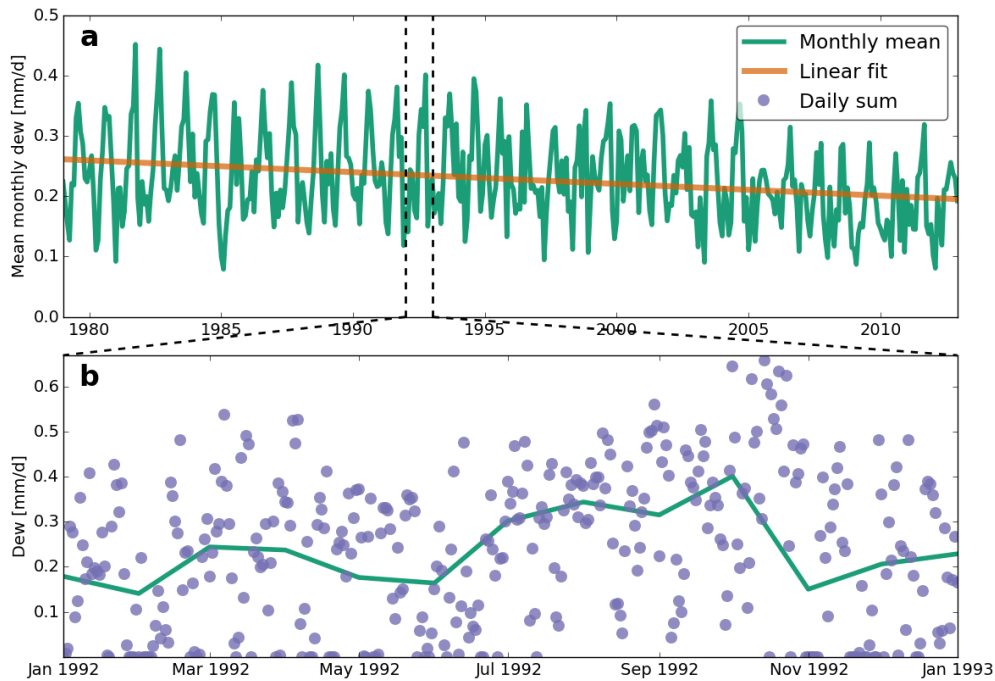
Figure 8. Time series of the modelled dew yield from one grid point, 30.75° N, 34.5° E, located in the Negev desert, Israel: **(a)** the monthly means over the whole data set, as well as a linear fit to the data; **(b)** the monthly means as well as daily values for the year 1992.
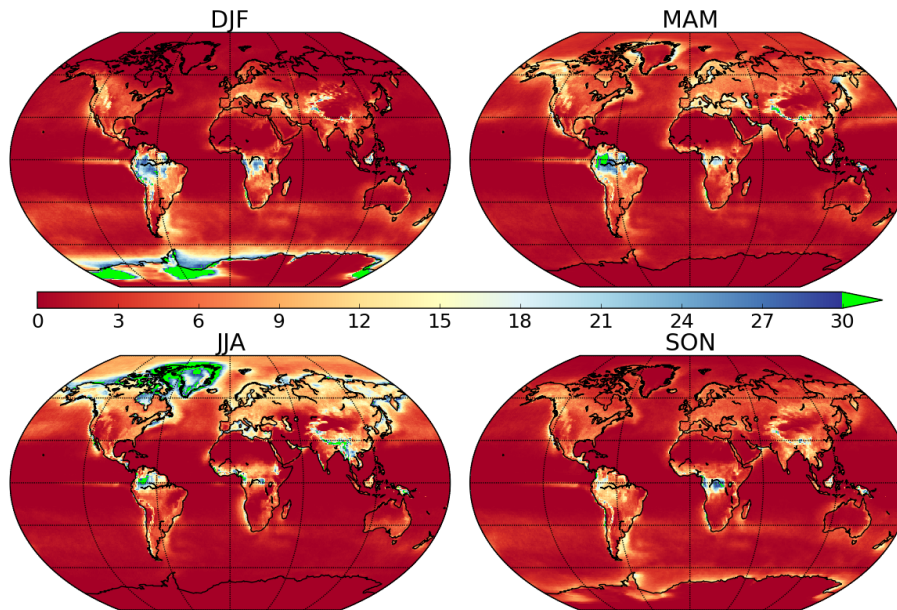

Figure 9. The fractional increase in the seasonal occurrence of dew (%) with a threshold of $0.1 \, \mathrm{mm \, d^{-1}}$, when the emissivity of the condenser is increased from 0.94 to 0.999, and the albedo from 0.84 to 0.999.

sula exhibit high standard deviations, suggesting that if large-scale dew collection in these areas was planned, varying dew yields should be expected.

Figure 8 presents a time series of dew yield in the Negev desert, Israel, where natural dew collection has been studied by several authors (e.g. Evenari, 1982; Zangvil, 1996;

Kidron, 1999; Jacobs et al., 2000). The values from our model are significantly higher than most of the reported values in other studies. However, this is expected since the majority of studies report yields of natural dew, which artificial surfaces typically outperform. In any case the coarse resolution of our data, as well as the differences in the collection
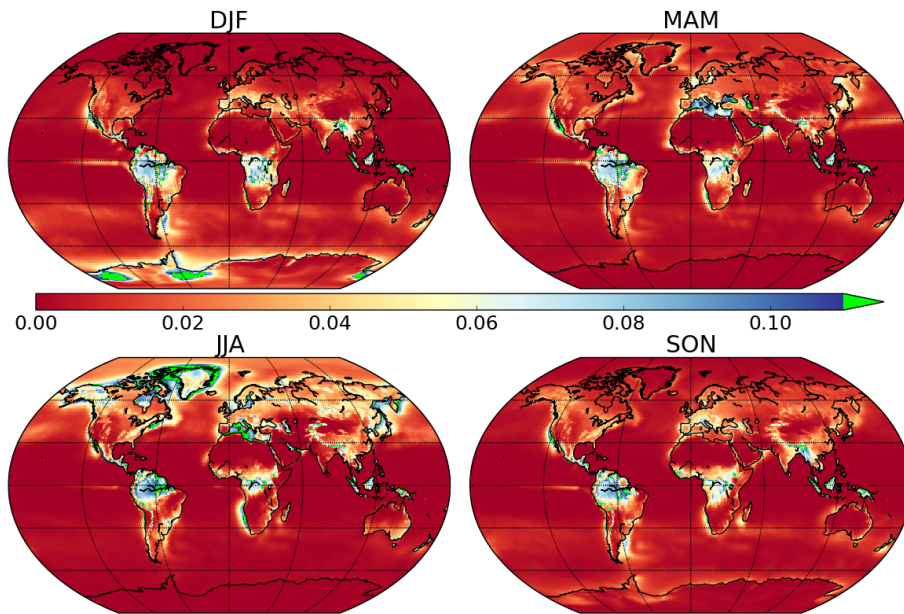
Figure 10. The absolute increase in the mean seasonal formation of dew ($mm\,d^{-1}$), when the emissivity of the condenser is increased from 0.94 to 0.999, and the albedo from 0.84 to 0.999.
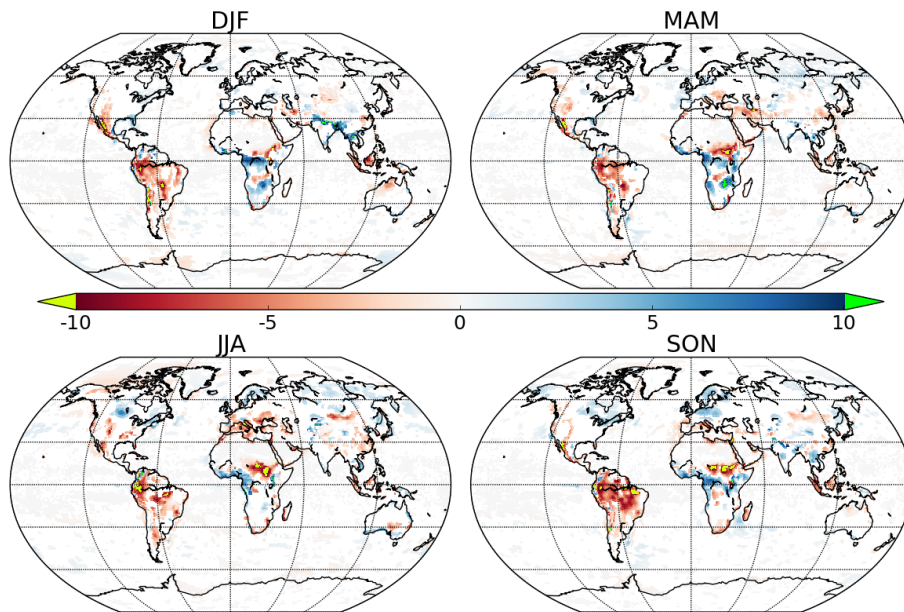

Figure 11. The total change (%) in the mean seasonal formation of dew ($mm\,d^{-1}$) over the years 1979–2012 as predicted by the Theil–Sen estimator. Only locations with a statistically significant trend ($p < 0.05$) are shown.

methods, make direct comparison with measurements difficult. Note the decreasing trend in the modelled dew yields in Fig. 8.

3.3 Increase of dew

The data presented in Fig. 5 are for a sheet emissivity of 0.94 and albedo of 0.84, both of which can possibly be im-

proved by means of material science. If both the emissivity and the albedo were hypothetically increased to an extreme value of 0.999, the occurrence of dew would increase as presented in Fig. 9. Although this *ideal collector* scenario is exaggerated, these model results suggest that improvements in the emissivity and albedo could have a significant effect on the sheet's ability to condense water, and thus the cost of a high-performance sheet material may be justified. It should

be noted that besides increasing the emissivity and the albedo of the sheet, other means of enhancing the condenser's performance exist as well. For example, Beysens et al. (2013) reported an increase in dew yields of up to 400 % for origami-shaped collectors compared to a planar condenser inclined at an angle of 30°.

In general, the ideal condenser scenario suggests that enhancing the properties of the condenser would increase the occurrence of dew most significantly over the summer-time Northern Hemisphere. In Antarctica and Greenland, the summer-time dew yields increase significantly over the subjective $0.1\,\mathrm{mm\,d^{-1}}$ limit in the ideal condenser scenario, which results in these regions being highlighted in Fig. 9.

The absolute increase in the mean seasonal formation of dew is presented in Fig. 10, suggesting that the dew yield can be more than doubled in some areas in this extreme scenario. In general, however, the increase in the absolute dew yield is relatively small even in areas where enhancing the condenser's properties significantly increases dew occurrence. This implies that the relative importance of different factors affecting dew formation varies globally, and that radiative cooling is the main limiting factor, for example, in the Mediterranean Sea.

3.4 Trend of dew

With the projected changes in climate and potentially increasing occurrences of drought (Stocker et al., 2013), we investigated the existence of temporal trends in the modelled dew yields. Trends were calculated by applying the Mann–Kendall (i.e. Kendall Tau-b) trend test (e.g. Agresti, 2010) on seasonal means of yearly data. Unsurprisingly, the statistical significance of the trends varies non-uniformly across the globe. Nevertheless, in many regions a statistically significant trend ($p < 0.05$) is found.

Figure 11 presents the overall change in the mean seasonal formation of dew. Only statistically significant ($p < 0.05$) changes are shown, with the trend being equal to the Theil–Sen estimator (Theil, 1950; Sen, 1968). Interestingly, the general trend appears to indicate a decrease in dew potential in most water-stressed areas. The changes appear in large and roughly uniform areas, suggesting that the phenomenon cannot be entirely attributed to noise. A significant decreasing trend is also visible in the case study presented in Fig. 8. In addition, a decreasing trend is also visible in parts of the coastal regions of northern Africa and the Arabian Peninsula, which we identified as regions of high dew collection potential (see previous sections).

4 Conclusions

The global potential for collecting dew on artificial surfaces was investigated by implementing a dew formation model based on solving the heat and mass balance equations. As meteorological input, 34 years of global reanalysis data from ECMWF's ERA-Interim archive was used.

Dew formation was found to be common and frequent, though mostly over land areas where other sources of water exist. Nevertheless, some water-stressed areas, especially parts of the coastal regions of northern Africa and the Arabian Peninsula, might be suitable for economically viable large-scale dew collection, as the yearly yield of dew may reach up to $100\,\mathrm{L\,m^{-2}}$ for a commonly used LDPE foil. For these locations, more accurate regional modelling and field experiments should be conducted.

The long time series provides some statistical confidence in conducting a trend analysis, and it suggests significant changes in dew yields in some areas up to and exceeding ±10 % over the investigated time period.

It should be noted that the real-life usefulness of the results presented in this paper depends on several factors not accounted for in this study, such as other sources of water (precipitation, lakes, rivers, desalination of seawater), pipelines, and road access to the location for transportation of water by trucks, as well as financial and technological considerations. Additionally, the uncertainties related to the transfer coefficients, the reanalysis data set and its near-surface application as well as the inherent uncertainties in any global modelling approaches should be acknowledged, and all numbers presented here are rough estimates only.

References

Agresti, A.: Analysis of ordinal categorical data, Vol. 656, John Wiley & Sons, New York, 2010.

Beysens, D.: The formation of dew, Atmos. Res., 39, 215–237, 1995.

Beysens, D., Muselli, M., Nikolayev, V., Narhe, R., and Milimouk, I.: Measurement and modelling of dew in island, coastal and alpine areas, Atmos. Res., 73, 1–22, 2005.

Beysens, D., Brogginib, F., Milimouk-Melnytchoukc, I., Ouazzanid, J., and Tixiere, N.: New Architectural Forms to Enhance Dew Collection, Chem. Eng., 34, 79–84, 2013.

Clus, O.: Condenseurs radiatifs de la vapeur d'eau atmosphérique (rosée) comme source alternative d'eau douce, PhD thesis, Université Pascal Paoli, 2007.

Decker, M., Brunke, M. A., Wang, Z., Sakaguchi, K., Zeng, X., and Bosilovich, M. G.: Evaluation of the reanalysis products from

GSFC, NCEP, and ECMWF using flux tower observations, J. Climate, 25, 1916–1944, 2012.

Dee, D. P., Uppala, S. M., Simmons, A. J., Berrisford, P., Poli, P., Kobayashi, S., Andrae, U., Balmaseda, M. A., Balsamo, G., Bauer, P., Bechtold, P., Beljaars, A. C. M., van de Berg, L., Bidlot, J., Bormann, N., Delsol, C., Dragani, R., Fuentes, M., Geer, A. J., Haimberger, L., Healy, S. B., Hersbach, H., Hólm, E. V., Isaksen, L., Kållberg, P., Köhler, M., Matricardi, M., McNally, A. P., Monge-Sanz, B. M., Morcrette, J.-J., Park, B.-K., Peubey, C., de Rosnay, P., Tavolato, C., Thépaut, J.-N., and Vitart, F.: The ERA-Interim reanalysis: configuration and performance of the data assimilation system, Q. J. Roy. Meteorol. Soc., 137, 553–597, 2011.

Evenari, M.: The Negev: the challenge of a desert, Harvard University Press, 1982.

Fessehaye, M., Abdul-Wahab, S. A., Savage, M. J., Kohler, T., Gherezghiher, T., and Hurni, H.: Fog-water collection for community use, Renew. Sustain. Energy Rev., 29, 52–62, 2014.

Jacobs, A., Heusinkveld, B., and Berkowicz, S.: Passive dew collection in a grassland area, the Netherlands, Atmos. Res., 87, 377–385, 2008.

Jacobs, A. F., Heusinkveld, B. G., and Berkowicz, S. M.: Dew measurements along a longitudinal sand dune transect, Negev Desert, Israel, Int. J. Biometeorol., 43, 184–190, 2000.

Jürges, W.: Der Wärmeüubergang an Einer Ebenen Wand, Beihefte zum Gesundheits-Ingenieur, 1, 1227–1249, 1924.

Kidron, G. J.: Altitude dependent dew and fog in the Negev Desert, Israel, Agr. Forest Meteorol., 96, 1–8, 1999.

King, M. D., Platnick, S., Menzel, W. P., Ackerman, S. A., and Hubanks, P. A.: Spatial and Temporal Distribution of Clouds Observed by MODIS Onboard the Terra and Aqua Satellites, Geoscience and Remote Sensing, IEEE Trans.. 51, 3826–3852, 2013.

Klemm, O., Schemenauer, R. S., Lummerich, A., Cereceda, P., Marzol, V., Corell, D., van Heerden, J., Reinhard, D., Gherezghiher, T., Olivier, J., Osses, P., Sarsour, J., Frost, E., Estrela, M. J., Valiente, J. A., and Fessehaye, G. M.: Fog as a fresh-water resource: overview and perspectives, Ambio, 41, 221–234, 2012.

Kumar, S., Sharma, V., Kandpal, T., and Mullick, S.: Wind induced heat losses from outer cover of solar collectors, Renew. Energy, 10, 613–616, 1997.

Lekouch, I., Lekouch, K., Muselli, M., Mongruel, A., Kabbachi, B., and Beysens, D.: Rooftop dew, fog and rain collection in southwest Morocco and predictive dew modeling using neural networks, J. Hydrol., 448, 60–72, 2012.

Lorenz, C. and Kunstmann, H.: The hydrological cycle in three state-of-the-art reanalyses: intercomparison and performance analysis, J. Hydrometeorol., 13, 1397–1420, 2012.

Madeira, A., Kim, K., Taylor, S., and Gleason, M.: A simple cloud-based energy balance model to estimate dew, Agr. Forest Meteorol., 111, 55–63, 2002.

Maestre-Valero, J., Martinez-Alvarez, V., Baille, A., Martín-Górriz, B., and Gallego-Elvira, B.: Comparative analysis of two polyethylene foil materials for dew harvesting in a semi-arid climate, J. Hydrol., 410, 84–91, 2011.

McAdams, W.: Heat Transmission, McGraw-Hill, New York, 1954.

Nikolayev, V., Beysens, D., Gioda, A., Milimouk, I., Katiushin, E., and Morel, J.: Water recovery from dew, J. Hydrol., 182, 19–35, 1996.

Nilsson, T.: Initial experiments on dew collection in Sweden and Tanzania, Solar Energy Mater. Solar Cells, 40, 23–32, 1996.

Nilsson, T., Vargas, W., Niklasson, G., and Granqvist, C.: Condensation of water by radiative cooling, Renew. Energy, 5, 310–317, 1994.

Onogi, K., Tsutsui, J., Koide, H., Sakamoto, M., Kobayashi, S., Hatsushika, H., Matsumoto, T., Yamazaki, N., Kamahori, H., Takahashi, K., Kadokura, S., Wada, K., Kato, K., Oyama, R., Ose, T., Mannoji, N., and Taira, R.: The JRA-25 reanalysis, J. Meteorol. Soc. JPN Ser. II, 85, 369–432, 2007.

Pedro, M. J. and Gillespie, T. J.: Estimating Dew Duration .1. Utilizing Micrometeorological Data, Agr. Meteorol., 25, 283–296, 1982.

Richards, K.: Adaptation of a leaf wetness model to estimate dewfall amount on a roof surface, Agr. Forest Meteorol., 149, 1377–1383, 2009.

Rienecker, M. M., Suarez, M. J., Gelaro, R., Todling, R., Bacmeister, J., Liu, E., Bosilovich, M. G., Schubert, S. D., Takacs, L., Kim, G.-K., Bloom, S., Chen, J., Collins, D., Conaty, A., da Silva, A., Gu, W., Joiner, J., Koster, R. D., Lucchesi, R., Molod, A., Owens, T., Pawson, S., Pegion, P., Redder, C. R., Reichle, R., Robertson, F. R., Ruddick, A. G., Sienkiewicz, M., and Woollen, J.: MERRA: NASA's Modern-Era Retrospective Analysis for Research and Applications, J. Climate, 24, 3624–3648, 2011.

Saha, S., Moorthi, S., Pan, H.-L., Wu, X., Wang, J., Nadiga, S., Tripp, P., Kistler, R., Woollen, J., Behringer, D., Liu, H., Stokes, D., Grumbine, R., Gayno, G., Wang, J., Hou, Y.-T., Chuang, H.-Y., Juang, H.-M. H., Sela, J., Iredell, M., Treadon, R., Kleist, D., Van Delst, P., Keyser, D., Derber, J., Ek, M., Meng, J., Wei, H., Yang, R., Lord, S., Van Den Dool, H., Kumar, A., Wang, W., Long, C., Chelliah, M., Xue, Y., Huang, B., Schemm, J.-K., Ebisuzaki, W., Lin, R., Xie, P., Chen, M., Zhou, S., Higgins, W., Zou, C.-Z., Liu, Q., Chen, Y., Han, Y., Cucurull, L., Reynolds, R. W., Rutledge, G., and Goldberg, M.: The NCEP climate forecast system reanalysis, B. Am. Meteorol. Soc., 91, 1015–1057, 2010.

Schemenauer, R. S. and Cereceda, P.: Fog-Water Collection in Arid Coastal Locations, Ambio, 20, 303–308, 1991.

Seinfeld, J. H. and Pandis, S. N.: Atmospheric Chemistry and Physics, John Wiley & Sons, New York, 2006.

Sen, P. K.: Estimates of the regression coefficient based on Kendall's tau, J. Am. Stat. Assoc., 63, 1379–1389, 1968.

Sharples, S. and Charlesworth, P.: Full-scale measurements of wind-induced convective heat transfer from a roof-mounted flat plate solar collector, Sol. Energy, 62, 69–77, 1998.

Simmons, A. J., Poli, P., Dee, D. P., Berrisford, P., Hersbach, H., Kobayashi, S., and Peubey, C.: Estimating low-frequency variability and trends in atmospheric temperature using ERA-Interim, Q. J. Roy. Meteorol. Soc., 140, 329–353, 2014.

Stocker, T. F., Qin, D., Plattner, G.-K., Tignor, M., Allen, S. K., Boschung, J., Nauels, A., Xia, Y., Bex, V., and Midgley, P. M.: Climate change 2013: The physical science basis, Intergovernmental Panel on Climate Change, Working Group I Contribution to the IPCC Fifth Assessment Report (AR5) (Cambridge Univ Press, New York), 2013.

Test, F., Lessmann, R., and Johary, A.: Heat transfer during wind flow over rectangular bodies in the natural environment, J. Heat Transf., 103, 262–267, 1981.

Theil, H.: A rank-invariant method of linear and polynomial regression analysis, Part 3, Proceedings of Koninalijke Nederlandse Akademie van Weinenschatpen A, 53, 1397–1412, 1950.

United Nations Development Programme: Human Development Report 2006, Beyond scarcity: Power, poverty and the global water crisis, Palgrave Macmillan, New York, 2006.

Watmuff, J., Charters, W., and Proctor, D.: Solar and wind induced external coefficients-solar collectors, Cooperation Mediterraneenne pour l'Energie Solaire, 1, 56, 1977.

Willett, K. M., Dolman, A. J., Hall, B. D., and Thorne, P. W. (Eds.): State of the climate in 2012, Vol. 94, Chap. Global Climate, S7–S46, B. Am. Meteorol. Soc., 2013.

Zangvil, A.: Six years of dew observations in the Negev Desert, Israel, J. Arid Environ., 32, 361–371, 1996.